Neuron, Volume *81*

Supplemental Information

Temporal Responses of *C. elegans* Chemosensory Neurons Are Preserved in Behavioral Dynamics

Saul Kato, Yifan Xu, Christine E. Cho, L.F. Abbott, and Cornelia I. Bargmann

FIGURE S1

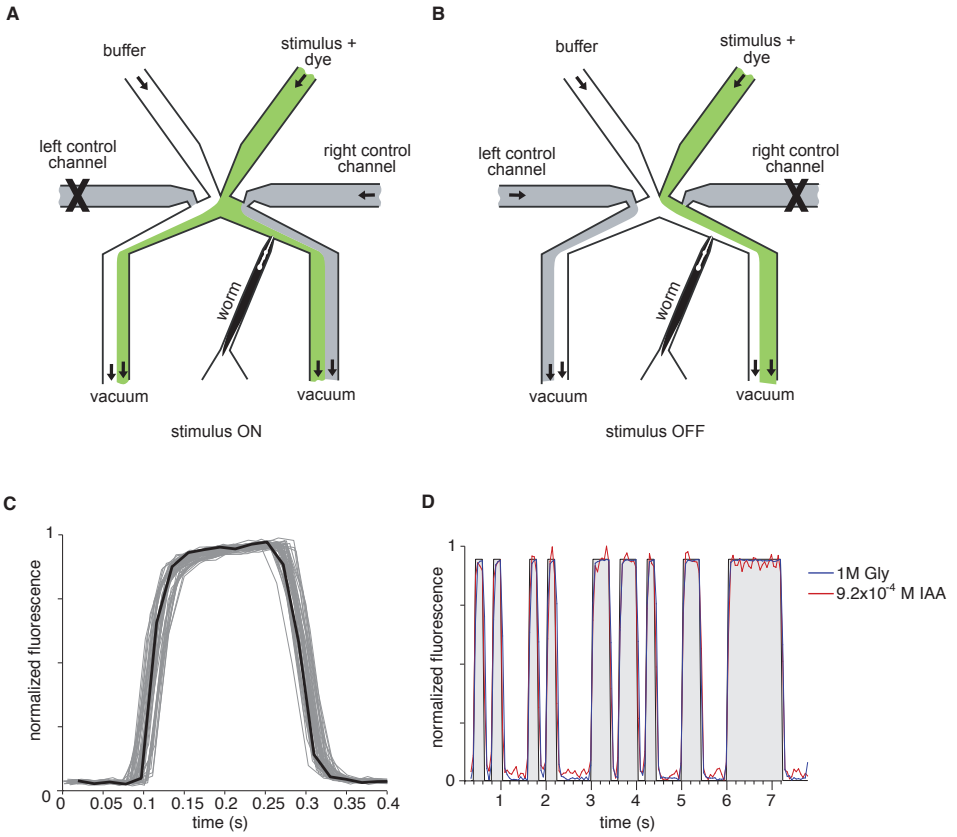

Figure S1 (related to Figure 1). Precise control of stimulus delivery.
(A, B) Chemical stimuli were delivered by switching between two laminar fluid streams that flowed across the nose of an adult hermaphrodite confined in a microfluidic chip **(Chronis et al., 2007)**. Delivery of sensory cues in liquid increases the speed and reliability of odor delivery and removal; *C. elegans* responds normally to chemical stimuli in all-liquid environments (**Luo et al., 2008; Albrecht and Bargmann 2011**). Schematic shows laminar fluid control by switching flow between side channels in a microfluidic chip during imaging. (A) Stimulus ON state showing stream of stimulus and fluorescein dye (green) flowing across worm nose. (B) Stimulus OFF state showing stream of buffer (white) flowing across worm nose.
(C) Control experiments with fluorescein dye in the stimulus stream showing that the system reliably delivered sequences of ON/OFF pulses at frequencies of up to 5 Hz. This corresponds to a switching rate that is roughly an order of magnitude more rapid than the fastest behavioral responses described in the Introduction. Graph, superposition of 50 consecutive time segments of normalized dye intensity for a 200 ms on/off square wave stimulus pattern,

recorded at a frame rate of 50 Hz. Individual segments shown in grey and mean intensity in black. Both off-on and on-off transitions were typically completed in ~50 ms.

(D) To accurately model the input-output transformation given the ~30 ms variability in switching time of the delivery system, fluorescein dye was included in the stimulus stream, and its intensity near the animal's nose was used as a surrogate for odor concentration during recordings. Graph shows representative normalized dye intensity during delivery of pseudo-random stimulus patterns of 1 M glycerol (blue) and 9.2×10^{-4} M isoamyl alcohol (red), superimposed over the electronic valve control signal. The reliability and transition time of the stimulus switching sequence were independent of the stimulus.

FIGURE S2

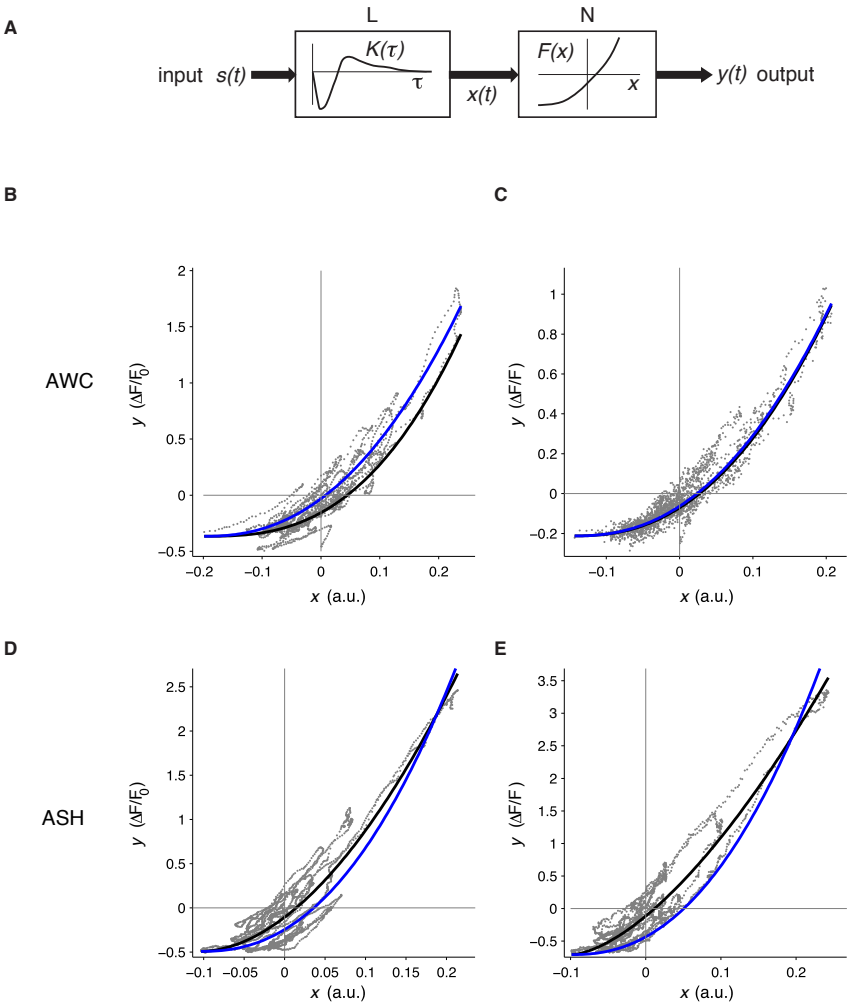

Figure S2 (related to Figure 3). The static nonlinearity of AWC and ASH responses approximates the nonlinearity of GCaMP3.

(A) Schematic of the L-N model. *K(τ)* describes a linear filter as a function of lag τ, and *F(x)* is an instantaneous function of the output from the linear filter. (B-E) Scatter plots of intermediate filtered signal *x(t)* versus output *y(t)* for L-N models composed from trial-averaged input-output records of AWC (B) and ASH (D), or representative individual m-sequence trials of AWC (C) and ASH (E), after linear filters and *x*(t) were estimated from input-output records. Black lines indicate the N power-law function least-squares fit to the scatter data. For comparison, blue curves indicate a power-law function fit to the scatter data with the power constrained to be 2.3, the Hill coefficient value for GCaMP3 reported in **Tian et al., 2009.**

FIGURE S3

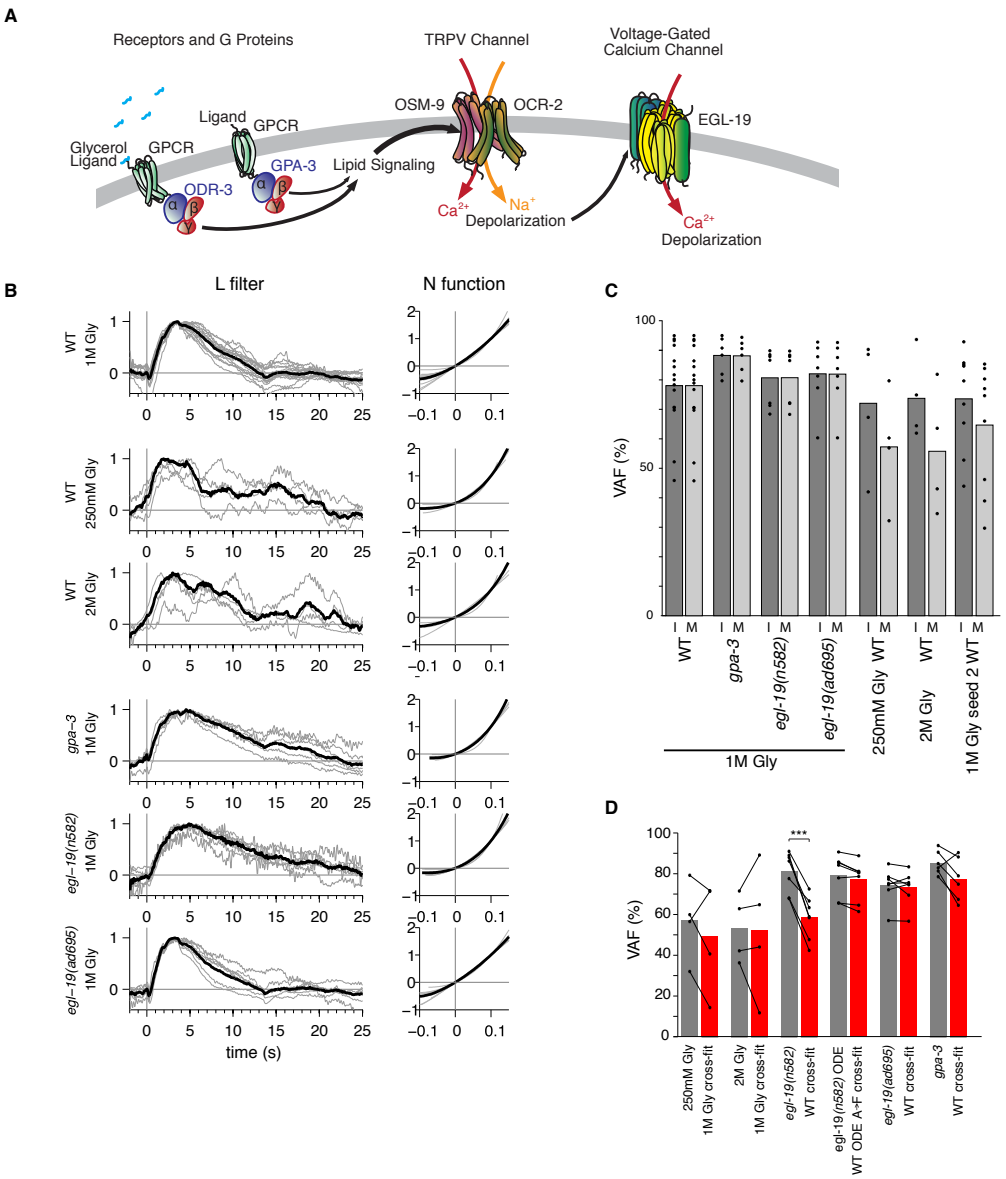

Figure S3 (related to Figures 2,5). Robustness of ASH wild type filters to concentration and m-sequence structure, and effects of signal transduction mutants.

(A) Signal transduction in ASH sensory cilia (**Bargmann, 2006**). The glycerol receptor is unknown, but is inferred to signal through the ODR-3 heterotrimeric G protein, which regulates TRPV family transduction channels. (B) Linear filters and nonlinear functions of L-N models extracted from m-sequence trials of wild type at different glycerol concentrations, and in mutants, showing individual trial filters (gray) and trial-averaged filters (black). L filters are normalized to the highest value, and expressed over time (sec). N function units are as in Figure S1D,E.

(C) Performance (% variance of accounted for) of individual trial L-N (denoted I) and mean trial-averaged L-N models (denoted M). WT 1M Gly, n=10; *gpa-3*, n=6, *egl-19(n582)*, n=7; *egl-19(ad695gf)*, n=7; WT 250mM, n=3; WT 2M, n=4; WT m-sequence seed 2, n=9. (D) Cross-condition performance (variance accounted for) of ASH reference filter (1M Gly, WT) or ASH WT A-F component only ODE model filter applied to input-output records using other concentrations or mutants. There is a significant difference between the *egl-19(n582)* and WT filters ($P<.001$, Welch's one-tailed t-test). Other cross-condition performance differences were not significant ($P>0.05$).

FIGURE S4

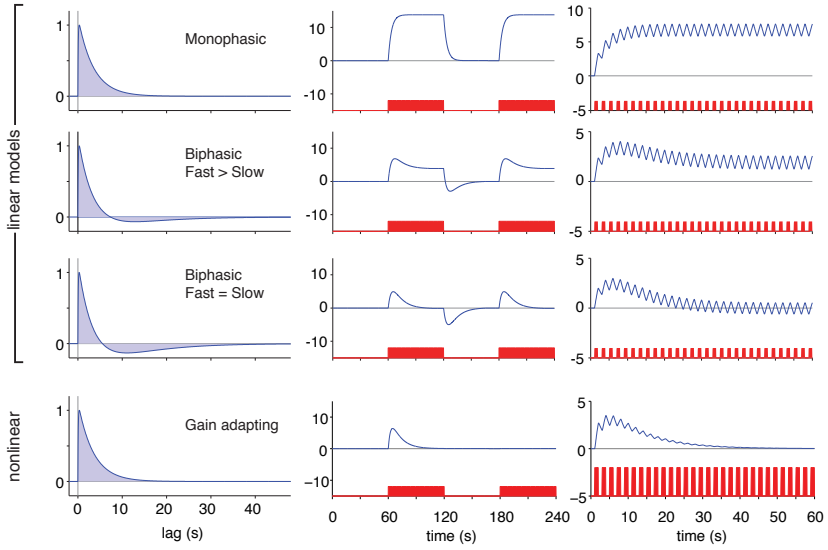

Figure S4 (related to Figure 4). Biphasic filters with distinct phase widths underlie many sensory responses.

First row: monophasic linear filter model corresponding to the AWC ODE model with the k_{as} parameter (see Figure 3B) set to zero. Second row: dual-timescale biphasic linear filter model with area of fast component greater than area of slow component, corresponding to the AWC ODE model. Third row: dual-timescale biphasic linear filter model with balanced phase area created by adjusting the AWC ODE parameters of k_{af} and k_{as} to give phases of equal area. Fourth row: monophasic filter model with nonlinear gain adaptation. The gain of the filter decays as a single exponential with time constant 10 s that starts at stimulus onset and does not recover.

Middle column: simulated responses of each model filter to 60 s pulse trains. Right column: simulated responses of each model filter to 1 s pulse trains.

The biphasic model in the second row captures both stimulus intensity and change, and is observed in other sensory mechanisms such as vertebrate phototransduction (**Schnapf et al., 1990**). Biphasic models in general (second and third rows) may be universal features of sensory processing, as they are observed across systems ranging from bacterial chemotaxis to human psychophysics (**Segall et al., 1986; Atick and Redlich, 1990;** Markus Meister, personal communication).

FIGURE S5

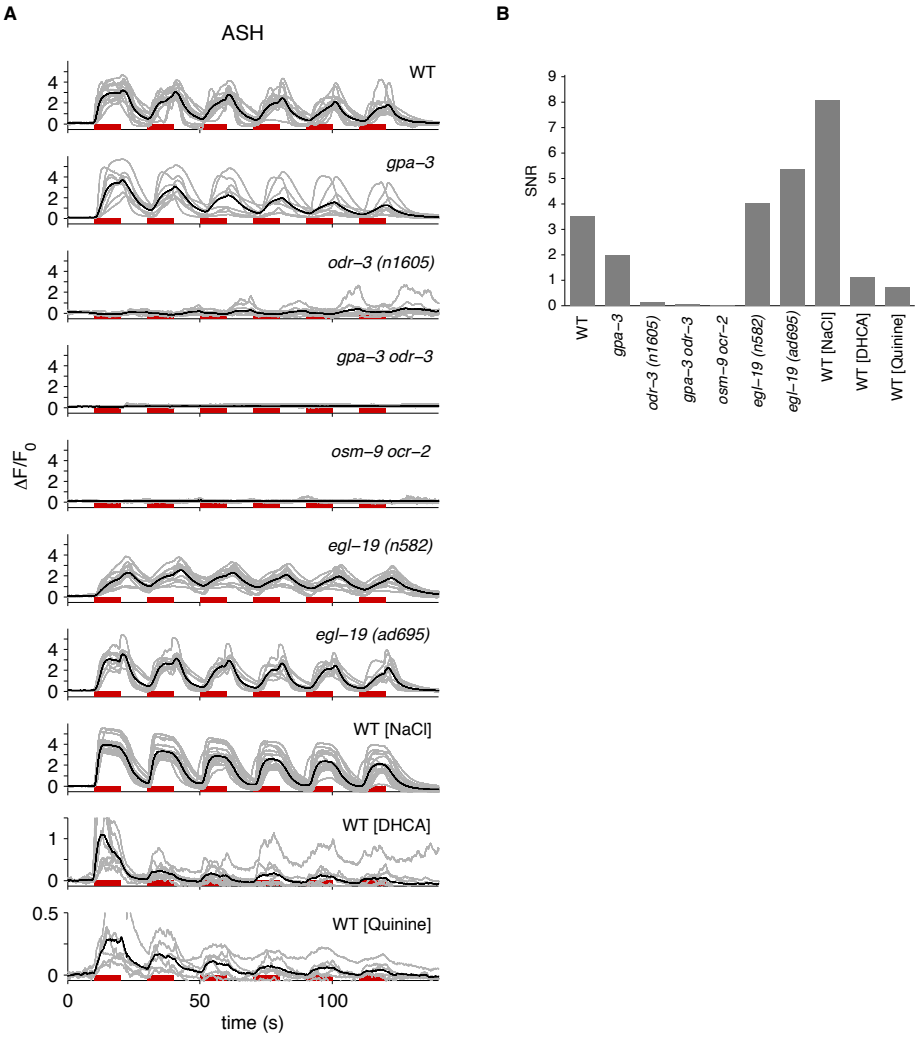

Figure S5 (related to Figures 4,5). ASH signal transduction mutant responses to 10 s stimulus pulses.

(A) Left column: ASH responses to six 10 s on/off pulses of 1 M glycerol (except where otherwise noted) in wild type and signal transduction mutants (wild type, n=12; *gpa-3,* n=10; *odr-3(n1605)*, n=10; *gpa-3 odr-3*, n=10; *osm-9 ocr-2*, n=14; *egl-19(n582)*, n=14; *egl-19(ad695gf)*, n=10; wild type using 500 mM NaCl, n=17; wild type using 300 mM DHCA, n=9; wild type using quinine, n=6). The *egl-19(n582)* glycerol response decays significantly less than the wild-type response across pulses.

(B) Signal-to-noise ratio of responses in (A), calculated as in **Sahani and Linden, 2003**.

FIGURE S6

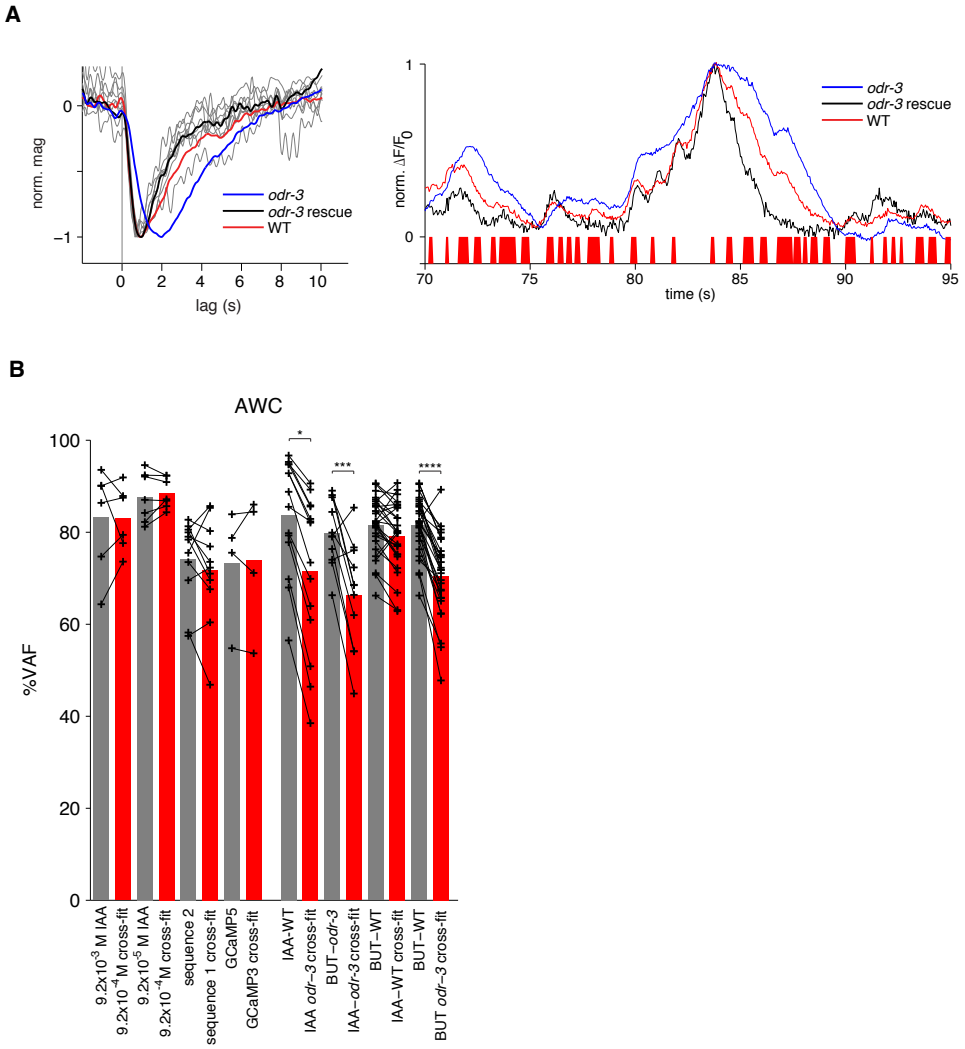

Figure S6 (related to Figure 4,6). AWC sensory filter dynamics in wild-type, *odr-3,* and *odr-3* rescued strains.

(A) A *Podr-3::odr-3* transgene rescues AWC filter dynamics of *odr-3(n2150)* mutants (n=8 animals each). Individual trial filters for *odr-3* rescue are shown in thin gray lines, and the trial average filter for *odr-3* rescue is shown in black. Shown at right are segments of wild-type, *odr-3*, and *odr-3* rescue normalized-to-peak responses to an m-sequence of $9.2x10^{-4}$ M isoamyl alcohol (IAA). The stimulus sequence is shown at bottom in red. The temporal resolution of the IAA-*odr-3* rescue response is as fine or finer than the IAA-WT response.

(B) Left group: cross-condition performance (variance accounted for) comparison of AWC reference filter ($9.2x10^{-4}$ M IAA, WT, m-

sequence 1, GCaMP3.0) as applied to input-output records using other concentrations, a second m-sequence, or GCaMP5A. There were no significant performance differences between groups (P>0.05).
Right group: cross-condition performance comparisons of (i) IAA-*odr-3* filter versus IAA-WT filter as applied to IAA-WT input-output records, (ii) IAA-*odr-3* versus BUT-*odr-3* filter as applied to BUT-*odr-3* input-output records, (iii) IAA-WT versus BUT-WT filter as applied to BUT-WT input-output records, and (iv) BUT-*odr-3* versus BUT-WT filter as applied to BUT-WT input-output records. IAA concentration was 9.2×10^{-4} M, BUT (butanone) concentration was 1.11×10^{-5} M. * P=.021, *** P=.0024 , **** P<.00001, Welch's one-tailed t-test. The BUT-WT versus IAA-WT performance difference was not significant (P>0.05).

TABLE S1, related to Figures 3,5

Parameter values of the ODE filter model (Figure 3B) fit to trial-averaged input-output records for various neurons and mutants.

Neuron	$1/k_a$ (s)	$1/k_f$ (s)	$1/k_s$ (s)	k_{as}/k_{af}
AWC	2.99	0.04	10.88	2.40E-03
ASH	3.59	4.10	5.92	5.56E-01
ASH *egl-19(n582)*	4.79	4.21	7.51	1.89E-01
ASH *egl-19(ad695gf)*	3.23	2.93	3.67	6.86E-01

Supplemental Experimental Procedures

C. elegans Cultivation and Strains

Strains were cultivated on agar plates seeded with *E. coli* strain OP50 at room temperature (~22°C). Standard methods for molecular biology were used. Strains used in this study are:

CX10979 *kyEx2865 [Psra-6::GCaMP3.0 + Pofm-1::gfp]*
CX13289 *odr-3(n1605) V*; *kyEx2865 [Psra-6::GCaMP3.0 + Pofm-1::gfp]*
CX13131 *gpa-3(pk35) V; kyEx2865 [Psra-6::GCaMP3.0 + Pofm-1::gfp]*
CX13132 *gpa-3(pk35) odr-3(n1605) V*; *kyEx2865 [Psra-6::GCaMP3.0 + Pofm-1::gfp]*
CX12739 *osm-9(ky10) ocr-2(ak47) IV; kyEx2865 [Psra-6::GCaMP3.0 + Pofm-1::gfp]*
CX13129 *egl-19(n582) IV; kyEx2865 [Psra-6::GCaMP3.0 + Pofm-1::gfp]*
CX13128 *egl-19(ad695gf) IV; kyEx2865 [Psra-6::GCaMP3.0 + Pofm-1::gfp]*
CX11935 *kyEx3252 [Pstr-2::GCaMP3.0+ Pofm-1::gfp]*
CX13838 *odr-3(n2150) V; kyEx3252 [Pstr-2::GCaMP3.0 + Pofm-1::gfp]*
CX15955 *odr-3(n2150) V; kyEx3252 [Pstr-2::GCaMP3.0 + Pofm-1::gfp]; kyEx5403 [Podr-3::odr-3cDNA::sl2::mCherry + Pelt-2::mCherry]*
CX13914 *kyEx4275 [Pstr-2::GCaMP5A + Pofm-1::dsRed]*

Neuronal Calcium Imaging and Analysis

Unless otherwise noted, stimuli were 1 M glycerol (ASH) or 9.2×10^{-4} M isoamyl alcohol (AWC), diluted in and alternating with S basal buffer. ASH imaging was preceded by a 90 s exposure to blue light to reduce its intrinsic light response (**Hilliard et al., 2005**). AWC imaging began after a 5 minute pre-exposure to odor, unless otherwise noted.

Stimulus presentation was automated using ValveBank (AutoMate Scientific) and LabJack interfaces to control a solenoid valve (LFAA1201610H, The Lee Company) with a pre-generated sequence. Switch time limitations were initially evaluated using 100 ms, 200 ms, 500 ms, 1 s, and 2 s flicker presentations for 5 minutes per trial to worms expressing GCaMP3 in ASH under the P*sra-6* promoter. Protocols using S basal buffer as background and either 1 M glycerol (with fluorescein) or S Basal buffer (with fluorescein) as the stimulus were used at each timescale to compare ASH calcium activity with stimulus onset. Measurement of fluorescein dye in the liquid stream near the worm's nose showed reliable square waves of dye fluorescence at 200 ms switch times.

Insignificant changes in ASH calcium signals were observed when the flickering stimulus switched between S basal and S basal with 1:250,000 dilution of fluorescein, allowing the use of fluorescein dye as a surrogate for odor concentration. Subsequent control experiments indicated that AWC and ASH calcium signals were insensitive to fluorescein inclusion with odor.

A Coolsnap HQ (Photometrics) camera controlled by Metamorph (Molecular Devices) software was used to capture stacks of TIFF images at 20 frames/sec during the odor presentation sequence. The average fluorescence intensity for a region of a particular cell was generated for each frame by averaging the pixel intensity of the brightest 100 pixels for soma recordings, or 10 pixels for axonal recordings, within a fixed bounding box surrounding the region of interest throughout the movie, then subtracting the average intensity of a 16 pixel background region adjacent to a corner of the bounding box. MATLAB (The Mathworks) was used for subsequent trace processing. Change in fluorescence intensity for the region of interest relative to F_0 was plotted for each trial individually, where F_0 was defined to be the average fluorescence in a 3 s window (t=1-4 s).

Trace Pre-Processing and Bleach Correction

Prior to model estimation, we pre-processed the traces to account for jitter in frame acquisition times and photobleaching. Jitter was corrected for by resampling each input and output record at regular time intervals at the intended frame rate of 20 s^{-1} using linear interpolation. When trial averaging was required, records were first time registered by shifting each record to have the same stimulus onset.

Bleach-corrected fluorescence traces were computed by transforming the measured fluorescence *F(t)*:

$$F_{corr}(t) = [F_{min}(0)/F_{min}(T)]^{t/T} F(t)$$

where $F_{min}(0)$ is the mean baseline fluorescence in the 2 s just before (set to be t=0) and $F_{min}(T)$ is the mean baseline fluorescence in the 2 s just after a stimulus sequence (t=T). To derive the bleach correction equation, we model photobleaching as a decay of sensitivity over time which affects all fluorescence levels as a multiplicative factor $B(t)=e^{-t/\tau}$. The parameter τ is determined by fitting *B(t)* through the points (1,0) and $(F_{\min}(T)/F_{\min}(0), T)$. This model of photobleaching

has the net effect of reducing both the baseline fluorescence and its dynamic range over time, an effect not incorporated into purely subtractive fluorescence bleach correction procedures.

As a final step prior to estimation, input-output records were trimmed to begin 45 s after initiation of the m-sequence stimulus to avoid non-stationarity due to the slowly decaying response to the initial stimulus offset or onset.

Linear-Nonlinear Model Estimation

Fully sampled linear filters *K* were estimated from pre-processed input-output records using least-squares regression. Filters were restricted to be 520 samples long, consisting of $T_+ = 40$ acausal and $T_- = 480$ causal samples. Trial-averaged filters were estimated by first trial-averaging pre-processed input and output records after jitter correction and time registration. Regression was performed by evaluating $\vec{K} = (U^T U)^{-1} U^T \vec{y}$ where $\vec{y}$ is a response record and *U* is a matrix with each row being a time-shifted copy of the corresponding input record *s*:

$$U = \begin{bmatrix} s(T_+) & \cdots & s(2) & s(1) & 0 & \cdots & 0 \\ s(T_+ + 1) & \ddots & s(3) & s(2) & s(1) & \cdots & 0 \\ \vdots & \cdots & \vdots & \vdots & \vdots & \cdots & \vdots \\ 0 & \cdots & s(N) & s(N-1) & s(N-2) & \ddots & s(N - T_-) \\ 0 & \cdots & 0 & s(N) & s(N-1) & \cdots & s(N - T_- + 1) \end{bmatrix}$$

Singular value decomposition was used to denoise *K,* using 100 components. Once an initial estimate of the linear filter *K*(t) was obtained, the associated instantaneous nonlinear function *F(x)* was estimated by least-squares fitting a power-law curve of the form $F(x) = a(x - x_{\min})^p + c$ to a scatter plot of intermediate signal values $x(t) = \int d\tau K(\tau) s(t-\tau)$ versus output values *y(t)*. The Nelder-Mead simplex method for nonlinear optimization was used to find the parameters *a*, *p*, and *c*. An iterative scheme was used to generate improved estimates of *K* and *F* by reducing bias error (**Hunter and Korenberg, 1986**). Model parameters did not change significantly after the second iteration.

Supplemental Text: Monitoring fast neuronal signals with genetically-encoded calcium indicators

The linear filters derived in this work describe the neuronal encoding of time-varying signals, and provide a framework for interpreting Ca^{2+} signal dynamics in *C. elegans* and in other systems in which genetically-encoded calcium indicators are increasingly used. The measured fluorescence signal encompasses odor diffusion to the cilia, receptor binding and unbinding, sensory signal transduction, its conversion into somatic calcium transients, and GCaMP calcium binding and fluorescence. Although we cannot separate all of these steps, we could correct for the GCaMP sensor analytically, and can make some inferences about the relative importance of other steps. For example, AWC cilia are partly embedded in a glial sheath, whereas ASH cilia are directly exposed to the environment. Therefore, the slower responses of ASH are likely to be a consequence of neuronal properties, not stimulus access. Odor-receptor binding kinetics are slower at lower odor concentrations, but the AWC filters are similar across a 100-fold odor concentration range, suggesting that receptor binding is not rate-limiting for this range. These considerations suggest that the filters measured here mainly report steps between receptor activation and calcium entry, including voltage changes.

System identification is widely used in electrophysiological studies, where it has shown considerable power to generate quantitative insights, but is only beginning to be applied to calcium imaging data (**Clark et al., 2011**). One question in interpreting these results is the extent to which calcium reflects neuronal activity. Since neurons regulate neurotransmitter release via presynaptic calcium, the correlations we observed between somatic and axonal (presynaptic) calcium dynamics in ASH and AWC support the analysis of somatic calcium as a slightly slowed surrogate for activity, at least under these conditions. A second question is whether the calcium sensors are fast enough to report endogenous signals, as they apparently were in these studies. Many *C. elegans* neurons function using slow graded potentials (**Goodman et al., 1998; Liu et al., 2009**), which may make them particularly suitable for using graded calcium signals as an activity measurement. It is encouraging that the current generation of genetically-encoded calcium indicators can follow single action potential spikes, which would make this approach possible for faster (mammalian) neurons as well (**Chen et al., 2013**).

Supplemental References

Chen, T.-W., Wardill, T.J., Sun, Y., Pulver, S.R., Renninger, S.L., Baohan, A., Schreiter, E.R., Kerr, R.A., Orger, M.B., Jayaraman, V., Looger, L.L., Svoboda, K., and Kim, D.S. (2013). Ultrasensitive fluorescent proteins for imaging neuronal activity. Nature *499*, 295-300.

Hunter, I.W., and Korenberg, M.J. (1986). The identification of nonlinear biological systems: Wiener and Hammerstein cascade models. Biol. Cybernetics *55*, 135-144.

Luo, L., Gabel, C.V., Ha, H.I., Zhang, Y., and Samuel, A.D. (2008). Olfactory behavior of swimming *C. elegans* analyzed by measuring motile responses to temporal variations of odorants. J. Neurophysiol. *99*, 2617-2625.

Sahani, M. and Linden, J. (2003). How linear are auditory cortical responses? Advances in Neural Information Processing Systems *15*, pp. 109-116, (Cambridge, MA: MIT Press).